PCCP

ROYAL SOCIETY OF CHEMISTRY

PAPER

Cite this: *Phys. Chem. Chem. Phys.*, 2022, **24**, 1424

Excited state photochemically driven surface formation of benzene from acetylene ices on Pluto and in the outer solar system†

N. Fabian Kleimeier, ‡[ab] Yiwei Liu, ‡[c] Andrew M. Turner,[ab] Leslie A. Young,[d] Chih-Hao Chin,[c] Tao Yang, *[ce] Xiao He, *[cf] Jen-lu Lo,[g] Bing-Ming Cheng[gh] and Ralf I. Kaiser *[ab]

Received 30th October 2021,
Accepted 19th December 2021

DOI: 10.1039/d1cp04959c

rsc.li/pccp

NASA's New Horizons mission unveiled a diverse landscape of Pluto's surface with massive regions being neutral in color, while others like Cthulhu Macula range from golden-yellow to reddish comprising up to half of Pluto's carbon budget. Here, we demonstrate in laboratory experiments merged with electronic structure calculations that the photolysis of solid acetylene – the most abundant precipitate on Pluto's surface – by low energy ultraviolet photons efficiently synthesizes benzene and polycyclic aromatic hydrocarbons *via* excited state photochemistry thus providing critical molecular building blocks for the colored surface material. Since low energy photons deliver doses to Pluto's surface exceeding those from cosmic rays by six orders of magnitude, these processes may significantly contribute to the coloration of Pluto's surface and of hydrocarbon-covered surfaces of Solar System bodies such as Triton in general. This discovery critically enhances our perception of the distribution of aromatic molecules and carbon throughout our Solar System.

Introduction

The New Horizons flyby of Pluto—the only trans-Neptunian Object (TNO) with a known atmosphere—transformed Pluto from an astronomical body into a geological world.[1] This mission uncovered exotic landscapes comprised of mountains of water ice (H_2O),[2] glaciers of frozen nitrogen (N_2),[3] dunes made of methane (CH_4) ice granules,[4] and vast basins like nitrogen ice dominated Sputnik Planitia.[1] Pluto's surface is reshaped by the sublimation of nitrogen, carbon monoxide (CO), and methane from the surface to the atmosphere.[5,6] At surface pressures of 1 Pa and temperatures of 37 K,[7] nitrogen dominates the atmospheric composition followed by methane with abundances of 0.3% in the lower regions and up to 18% in the upper atmospheric layers above 1000 km. The absorption of solar photons by methane and nitrogen causes a complete opacity of the atmosphere at wavelengths of 142.5 nm and below.[7–9] This leads to photochemically generated hydrogen cyanide (HCN, 4×10^{-5})[10] together with C2 hydrocarbons acetylene (C_2H_2), ethylene (C_2H_4), ethane (C_2H_6), each at fractions of about 0.1%.[11–13]

Pluto's most prominent surface topographies are monumental colored terrains.[14] These stretch from black to reddish regions such as Cthulhu Macula extending over nearly 3000 km along Pluto's equator to yellowish topologies like Lowell Regio and Sputnik Planitia.[15] Whereas related terrestrial structures are composed of minerals, on Pluto, visible and near infrared images (1.25–2.50 μm) from New Horizons' Ralph instrument indicate strong fractions of dark organics—presumably tholin-like macro molecules[16]—of hitherto poorly characterized chemical composition and origin.[17] Considering areal mass fractions of up to 54% of organic molecules in Sputnik Planitia,[17] these strongly colored regions define the dominant surface sink of carbon in Pluto's nitrogen–methane cycle. Given

[a] *W. M. Keck Research Laboratory in Astrochemistry, University of Hawaii at Manoa, Honolulu, HI 96822, USA. E-mail: ralfk@hawaii.edu*
[b] *Department of Chemistry, University of Hawaii at Manoa, Honolulu, HI 96822, USA*
[c] *State Key Laboratory of Precision Spectroscopy, Shanghai Engineering Research Center of Molecular Therapeutics and New Drug Development, School of Chemistry and Molecular Engineering, East China Normal University, Shanghai 200062, P. R. China. E-mail: tyang@lps.ecnu.edu.cn*
[d] *Southwest Research Institute, Department of Space Studies, Boulder, CO 80302, USA*
[e] *Collaborative Innovation Center of Extreme Optics, Shanxi University, Taiyuan, Shanxi 030006, P. R. China*
[f] *New York University – East China Normal University Center for Computational Chemistry, New York University, Shanghai 200062, P. R. China. E-mail: xiaohe@phy.ecnu.edu.cn*
[g] *Department of Medical Research, Hualien Tzu Chi Hospital, Buddhist Tzu Chi Medical Foundation, Hualien City 970, Taiwan*
[h] *Tzu-Chi University of Science and Technology, Hualien City 970, Taiwan*
† Electronic supplementary information (ESI) available. See DOI: 10.1039/d1cp04959c
‡ These authors contributed equally to this work.

that these organic molecule-dominated territories profoundly influence Pluto's hydrocarbon balance and climate on a planetary scale, the untangling of the origin and chemical pathways to organic materials is essential not only to rationalize Pluto's chemical evolution, but also to elucidate how alike and distinct the chemistries of Pluto and Earth might have been before life emerged on Earth 3.7 billion years ago.

Previous work has concentrated on the formation of the (colored) surface organics in the atmosphere through processing of methane (CH_4) and nitrogen (N_2) *via* solar photons. These photochemically driven molecular mass growth processes involve complex gas phase reaction networks of ion–molecule and neutral–neutral reactions,[12,13] eventually leading to haze layers of organic aerosol particles.[8,18] Hydrocarbons can stick to these aerosol particles well above their condensation temperature[13] and eventually precipitate onto Pluto's surface.[11,12] Analyses of the opacity and scattering of Pluto's haze indicate that the aerosols are dominated by organics of unknown chemical makeup forming 10 nm particles that aggregate into particles of sizes up to 200 nm.[8,19] However, the hypothesis of precipitated aerosols as a source of the coloration of Pluto's yellowish to brownish surfaces has come under close examination. Recent photochemical models reveal that the residence time of the haze particles in Pluto's atmosphere of only three terrestrial years is too short to allow an adequate chemical processing and hence coloration of the organics prior to their precipitation to the surface.[15,20] One possible explanation for the coloration is the possibility of a seasonal collapse of the atmosphere allowing Ly-α photons and solar wind particles to reach the surface and induce coloration,[18] however, seasonal and long-term models indicate that the methane concentration in the atmosphere rarely turns out to be small enough for the atmosphere to become transparent to this radiation.[21,22] Therefore, the severe discrepancy of the required and actual residence time of the aerosols suggests an alternative source of the surface organics indicating hitherto unidentified chemical processes on Pluto's surface.

Here we reveal *via* surface-science experiments merged with high-level *ab initio* calculations that benzene (C_6H_6)—the fundamental molecular building block of polycyclic aromatic hydrocarbons (PAHs)—along with substituted PAHs as complex as $C_{26}H_{24}$ are formed through photochemical processing of low temperature acetylene (C_2H_2) ices at wavelengths shorter than 288 nm *via* (non-adiabatic) excited state chemical dynamics. These previously ignored non-equilibrium pathways involve excited state photodynamics and may represent the key reaction class that results in the facile formation of colorful aromatic molecules ranging from yellow-orange (tetracene, $C_{18}H_{12}$) *via* golden-brown (perylene, $C_{20}H_{12}$) to red (ovalene, $C_{32}H_{14}$) similarly to the colors observed in distinct regions on Pluto such as Cthulhu Macula (red) or Lowell Regio and Sputnik Planitia (golden yellow),[15,16] on time scales as short as a few Earth years (ESI†). Photochemical models of Pluto's atmosphere converge that acetylene (C_2H_2) represents the most abundant molecule precipitating on Pluto's surface with fractions of up to 41%.[11,12] Pluto's low surface temperature of only 37 K effectively prohibits a classical thermal chemistry, but supports chemical processing by energetic radiation. High-energy Galactic Cosmic Rays (GCRs) with energies of at least a few MeV can penetrate the atmosphere[15] and deliver doses of up to 9×10^{-6} eV molecule^{-1} over Pluto's orbit (248 years) to the surface.[23] Solar photons at wavelengths less than 142.5 nm are absorbed in the atmosphere by methane, nitrogen, and the haze and, hence, do not reach the surface.[7,9,11,15] Nonetheless, low energy Solar Photons (142.5–290 nm; 8.7–4.3 eV) reach the surface[8,24] and deposit a dose of up to 14.5 eV per (acetylene) molecule during Pluto's orbit when accounting for daytime irradiation only. This exceeds the dose delivered by GCRs by at least six orders of magnitude. However, due to the low solar emission of photons that can penetrate the atmosphere and drive radical–radical chemistry (5.8–8.7 eV), these account for only 10% of this dose despite the higher absorption cross section. Previous atmospheric models deemed the dominating low-energy photons with energies below typical carbon–hydrogen bond energies and adiabatic ionization energies of, *e.g.*, acetylene as photochemically irrelevant since they can lead neither to bond cleavages nor ionization. Likewise, excited state photochemistry of low-lying electronic states of organics such as of acetylene was not part of any photochemical model of Pluto.[25] Overall, this low-energy (4.3–5.8 eV) photon-driven surface chemistry has the unique potential to efficiently transform acetylene ices over geologically short time scales through molecular mass growth processes to benzene and more complex aromatics of various degrees of coloration. Since our studies reveal that coloration takes place within a few Earth years, this time scale might even be sufficiently fast to cause coloration of acetylene-dominated haze particles before they settle on Pluto's surface (ESI†). These processes deliver the fundamental molecular building blocks not only for Pluto's surface organics, but potentially also for organic molecules on surfaces of Solar System bodies with dense atmospheres such as Titan thus providing a versatile, previously overlooked mechanistic framework for the synthesis of complex organic molecules of various degrees of coloration as ubiquitous in our Solar System.

Experimental

The experiments were carried out in a stainless steel ultrahigh vacuum (UHV) chamber with background pressures around 3×10^{-11} torr.[26] A polished, highly reflective silver substrate was interfaced to a closed-cycle helium refrigeration unit capable of reaching temperatures down to 5 K. Excellent thermal contact between the cold head and the silver substrate was ensured by sandwiching indium foil. Utilizing a differentially pumped rotational feedthrough and a UHV bellow, the cold head can be moved vertically and rotated horizontally. Acetylene (Airgas, 99.99% purity) was separated from the acetone stabilizer using a slush bath of dry ice and ethanol to freeze out the acetone. The purified acetylene gas was then deposited through a glass capillary array onto the silver substrate held at 5 K. During deposition, a helium-neon laser was reflected off the silver surface to record interference fringes to determine the

thickness of the ice.[27] With a refractive index of 1.34,[28] the thickness of the prepared ices was determined to 1200 ± 100 nm for the experiments carried out with 288 nm and 249 nm laser irradiation and 1000 ± 100 nm for the 222 nm experiment. Following the deposition, an IR spectrum was recorded (Nicolet 6700; 4500–700 cm^{-1}, resolution 4 cm^{-1}) before the ice was irradiated with a 1 cm^2 laser beam at normal incidence with average powers of about 15 mW. The resulting total energy of the laser impinging on the surface as well as the doses the ices received are summarized in Table S1 (ESI†). After irradiation, FTIR spectroscopy was exploited to detect changes in the chemical composition of the sample.

After the irradiation of the ice, the sample was warmed up to 320 K at a rate of 0.5 K min^{-1} (Temperature Programmed Desorption; TPD) to release volatile product molecules into the gas phase. Subliming species were subsequently ionized using a [1 + 1] REMPI scheme; the resulting ions were detected in a reflectron time-of-flight spectrometer (Jordan-TOF products, Inc.) equipped with two microchannel plates (MCPs) in a chevron geometry. The signal from the MCPs was amplified (Ortec 9306) and shaped in a discriminator with 100 MHz to finally be recorded with a multichannel scaler (FAST ComTec, P7888-1E); this unit was triggered at 30 Hz with a digital delay-pulse generator (Quantum Composers, 9518) and synchronized with the ionization laser. Each spectrum was integrated over 3600 sweeps, corresponding to one mass spectrum per Kelvin temperature change. The laser radiation used for the [1 + 1] REMPI scheme was generated in a dye laser (Sirah Lasertechnik GmbH, Cobra Stretch) pumped by the third harmonic (355 nm) of a Nd:YAG laser operating at 30 Hz (Spectra-Physics, Quanta-Ray Pro-250). To achieve an output of around 259 nm, a Coumarin 503 (Luxottica Exciton) dye solution was used and the laser was tuned to 518 nm which was subsequently frequency doubled in a BBO crystal. To find the exact wavelength needed, a separate experiment was conducted in which acetylene ice was irradiated with 5 keV electrons, which has previously been demonstrated to form benzene.[29] During the TPD phase, the laser was scanned over the relevant wavelength range and the wavelength was determined using a wave meter (Coherent, Wavemaster). In this scan, 259.003 nm was found to produce the strongest signal and was therefore used in the laser irradiation experiments (Fig. S8, ESI†). This wavelength can excite benzene to it first excited state, from which a second photon is sufficient to ionize the molecule. To avoid saturation of the signal after 222 nm irradiation, the MCP voltage was reduced to a detection efficiency of about 9.5% of the efficiency during the other experiments. This efficiency was determined by flooding the main chamber with defined pressures of gaseous benzene and recording the signal at different MCP voltages (Fig. S9, ESI†). To irradiate the acetylene ice, a second dye laser pumped by the second (for 288 nm) or third harmonic of a Nd:YAG laser operating at 30 Hz (Spectra-Physics, Quanta-Ray Pro-270). For each wavelength, the output of the dye laser was frequency doubled in a BBO crystal. Dyes used were Pyrromethene 597, Coumarin 503, and Coumarin 450 for 288 nm, 249 nm, and 222 nm, respectively. An additional experiment with irradiation at 222 nm was carried out on a rhodium-coated silver substrate to collect UV-Vis data of the processed sample without the strong absorption of silver in the UV region. Spectra were taken from 190–1100 nm at a resolution of 4 nm (Nicolet Evolution 300).

The transmission spectrum of acetylene ice was measured from 107 nm to 350 nm at a VUV absorption end station attached to the beam line BL03 at the 1.5 GeV Taiwan Light Source (TLS) in the National Synchrotron Radiation Research Center (NSRRC) of Taiwan. The generated light is dispersed with a 6 m cylindrical grating monochromator and spans the wavelength range 35–350 nm with a maximum photon flux of about 2×10^{12} photons s^{-1} and a maximum resolving power of 30 000. A LiF, CaF_2 or quartz window plate was inserted at the front of the end-station to remove the higher-order light from the beamline. The experimental setup was described previously.[30,31] In short, acetylene (Matheson, 99.99% purity) was separated from the stabilizer in a cold trap at 195 K and a thin film was deposited onto a 2 mm thick LiF window held at 10 K using a closed-cycle helium refrigerator (APD HC-DE204S) in a vacuum chamber at pressures below 10^{-8} torr. Monochromatized radiation from the synchrotron was passed through a gold mesh with 90% transmission to monitor the flux using an electrometer (Keithley 6512). After passing through the acetylene ice and the LiF window at normal incidence, the synchrotron radiation was absorbed by a layer of sodium salicylate coated onto a glass window. The phosphorescence of the salicylate was monitored using a photomultiplier tube (Hamamatsu R943-02) in photon-counting mode.

Computations

Structures of the reactants, intermediates, transition states, and products at the first excited triplet state (T_1) were obtained using the hybrid density functional B3LYP[32] with the 6-311G** basis set. At the same computational level, vibrational frequencies were calculated to confirm the local minima with all positive frequencies and transition states with only one imaginary frequency. Intrinsic reaction coordinate (IRC) calculations were performed at the B3LYP/6-311G** level to verify that the optimized geometry is truly a transition state, which connects the designated intermediates. Subsequently, single-point energy calculations were carried out with the high-level wavefunction theories based on the B3LYP/6-311G** optimized T_1 geometries. Second-order Møller–Plesset perturbation theory (MP2), and the coupled cluster with single, double and perturbative triple excitations (CCSD(T)) method[33] with extrapolation to the complete basis set (CBS) limit were performed to obtain the relative energies. The zero-point energies were corrected using B3LYP/6-311G**, and the solvation energy was calculated by the conductor-like polarizable continuum (CPCM) model with B3LYP/6-311G** for the T_1 C_6H_6 potential energy surface. The expressions used for the CCSD(T)/CBS calculation are as follows, where $E^c(MP2/CBS_{2,3})$ is the extrapolated MP2 correlation energy using the cc-pVDZ and cc-pVTZ basis sets and the extrapolation approach.[34] These CCSD(T)/CBS calculations were employed to predict relative energies of all reactants, intermediate states, transition states and products to a precision

of about 5 kJ mol^{-1}. All the quantum mechanical calculations were performed using Gaussian09[35] and MOLPRO.[36]

$$\begin{aligned} E(\mathrm{CCSD(T)/CBS}) &= E(\mathrm{HF/cc\text{-}pVQZ}) + E^{c}(\mathrm{MP2/CBS_{2,3}}) \\ &+ E^{c}(\mathrm{CCSD(T)/cc\text{-}pVDZ}) \\ &- E^{c}(\mathrm{MP2/cc\text{-}pVDZ}) \\ &+ \mathrm{ZPE(B3LYP/6\text{-}311G^{**})} \\ &+ E_{\mathrm{CPCM}}(\mathrm{B3LYP/6\text{-}311G^{**}}) \end{aligned} \quad (1)$$

$$\begin{aligned} E^{c}(\mathrm{MP2/CBS_{2,3}}) &= [3^{3}E^{c}(\mathrm{MP2/cc\text{-}pVTZ}) \\ &- 2^{3}E^{c}(\mathrm{MP2/cc\text{-}pVDZ})]/(3^{3} - 2^{3}) \end{aligned} \quad (2)$$

Structures of the reactants, intermediates, transition states, and products at the second excited triplet state (T_2) were optimized using the linear-response time-dependent density functional theory (LR-TDDFT) at the TD-B3LYP/6-311G** level. All TDDFT calculations were carried out with Gaussian16.[37] Next, single-point energies of the TD-B3LYP/6-311G** optimized T_2 states were calculated by the complete active-space second-order perturbation theory (CASPT2)[38] with the aug-cc-pVTZ basis set using MOLPRO.[36] The zero-point energies were corrected with TD-B3LYP/6-311G**, and the solvation energy was calculated by the CPCM model at the TD-B3LYP/6-311G** level for the T_2 state C_6H_6 potential energy surface.

Results

In separate experiments ices of acetylene (C_2H_2) were irradiated by monochromatic photons with wavelengths of 288 nm (4.31 eV), 249 nm (4.98 eV), and 222 nm (5.58 eV) at 5 K. These photon energies are below the carbon-hydrogen bond strength (5.781 ± 0.030 eV)[39] and the first adiabatic ionization energy of acetylene (11.40 ± 0.05 eV)[40] thus eliminating, for instance, any ion chemistry.[41,42] Considering adiabatic excitation energies of the first excited triplet (T_1; 3.8 eV and 4.1 eV for *cis* and *trans*, respectively), second excited triplet (T_2; 4.7 eV and 4.4 eV), and first excited singlet state (S_1; 5.5 and 5.09 eV),[43–45] these wavelengths were chosen to investigate the influence of excited states on the low-temperature processing of acetylene (Fig. 1). As demonstrated in Fig. 2, a thin film of 1,330 ± 80 nm as determined using the Swanepoel method[46] (ESI†) of acetylene absorbs 0.10 ± 0.01%, 0.28 ± 0.03% and 0.55 ± 0.06% of the impinging photons, respectively, corresponding to absorptions of 3.9 ± 0.4 × 10^{-22}, 1.1 ± 0.1 × 10^{-21} and 2.2 ± 0.2 × 10^{-21} molecule^{-1}. In these experiments, ices received doses of 1.7 ± 0.2, 4.3 ± 0.7, and 8.4 ± 1.2 eV molecule^{-1} at 288 nm, 249 nm, and 222 nm, respectively (Table S1, ESI†). This corresponds to 32 ± 4, 82 ± 13, and 160 ± 20 Earth-years of irradiation on Pluto's surface. After the photolysis, the ices were warmed up to 300 K [temperature programmed desorption (TPD)] to release the molecules into the gas phase. We acknowledge that the temperature of Pluto never exceeds 110 K;

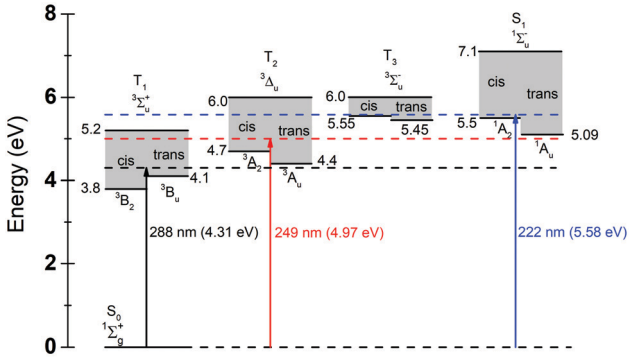

Fig. 1 Energy level diagram of the four lowest energy excited states. The upper energy limit of each state corresponds to the linear symmetry (vertical excitation), the lower lines to the adiabatic transitions to the *cis* and *trans* geometries. Arrows and dashed lines correspond to the excitation energies used in this study.

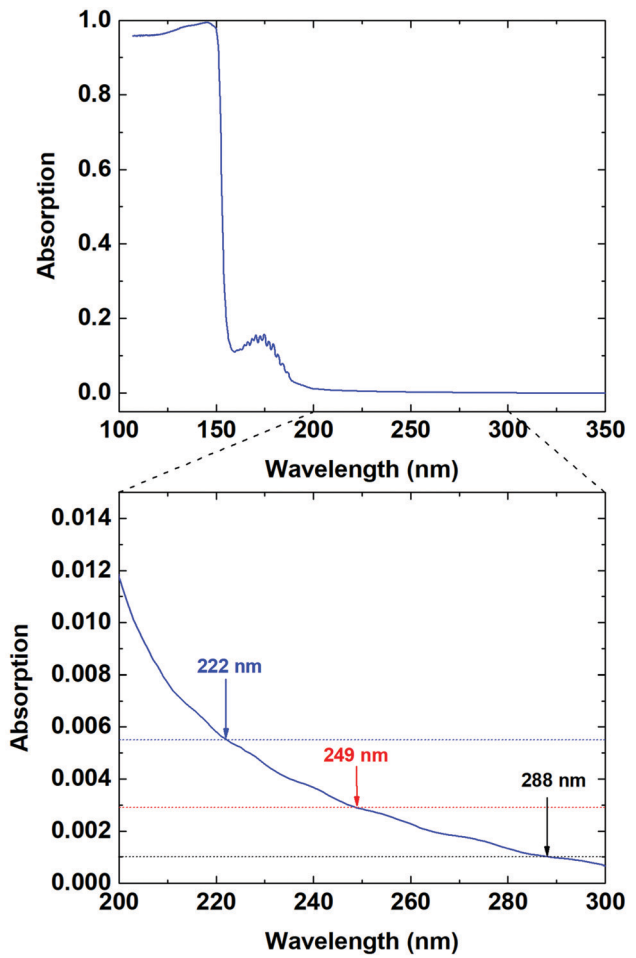

Fig. 2 Absorption spectrum of solid acetylene from 107 to 350 nm. The bottom panel shows an enlarged view of the wavelength range from 200 to 300 nm. Arrows indicate the wavelengths used in this study.

however, the warm-up phase is required to sublime the molecules into the gas phase, where they can be detected *via* photoionization through resonance-enhanced multiphoton ionization (REMPI)

followed by a mass-resolved detection of the aromatic molecules in a reflectron time-of-flight mass spectrometer (ReToF-MS).[29,47] REMPI-ReToF-MS is critical to identify individual molecules; traditional spectroscopies such as Fourier transform infrared (FTIR) and ultraviolet-visible (UV-vis) spectroscopy monitor functional groups linked to aromatics, but they often cannot assign individual molecules since the fundamental modes often overlap.[29] Acetylene ices were selected as the dominant components of all organics depositing on Pluto's surface from the atmosphere.[11,12] Therefore, they serve as a benchmark to what extent aromatic molecules and in particular benzene formed *via* low-temperature surface processing by low energy photons previously deemed irrelevant to synthesize any organics on hydrocarbon-rich surfaces of planets and their moons.

FTIR/UV-vis spectra

Representative FTIR spectra of acetylene ice before (black line) and after (red line) photolysis with 222 nm photons are displayed in Fig. 3. Before irradiation, the absorptions can be connected to acetylene. The main absorptions of the unprocessed ice can be assigned to the acetylenic ≡CH stretch (ν_3; 3235 cm^{-1}), a combination band ($\nu_4 + \nu_5$; 1391 cm^{-1}), and the C≡C–H bending mode (ν_5; 784/743 cm^{-1}).[28] An overview of all absorptions of the ice is given in Table S2 (ESI†). After the photolysis, several new, but weak bands can be identified as revealed in the insets of Fig. 3 (Table S3, ESI†). Most prominently, a combination band ($\nu_{16} + \nu_{13}$; 3089 cm^{-1}), a C=C stretch (ν_{13}; 1477 cm^{-1}), and a C–H bending mode (ν_{12}; 1035 cm^{-1}) might be linked to benzene (C_6H_6), but also to higher order aromatics.[48] Additionally, vinylacetylene (C_4H_4) can be identified by its acetylenic ≡CH stretch (ν_1; 3287 cm^{-1}) and a combination band ($\nu_6 + \nu_7$; 2970 cm^{-1}).[49] Furthermore, aromatic =CH stretches are detected at 3065 cm^{-1} and 3035 cm^{-1} indicating the formation of key functional groups of PAHs upon photolysis; this is further confirmed through broad absorptions around 997 and 959 cm^{-1} corresponding to in-plane and out-of-plane aromatic CH deformations of PAHs and (substituted) benzene, respectively. These substitutions are further indicated by the detection of alkyl CH stretching at 2925 cm^{-1}, alkane –CH_2– stretching at 2840 cm^{-1} and alkyne C≡C stretching at 2117 cm^{-1}. Since the infrared absorptions of PAHs often overlap due to their aromatic functional group, any assignments of specific molecules exploiting FTIR data alone must be considered as tentative. Further, the UV-Vis spectra recorded for the 222 nm irradiation experiment do not exhibit notable features, but reveal an increase in absorption over the whole spectral range from 190 nm to 1100 nm which is most pronounced in the UV and blue spectral region, indicating a yellow coloration compared to the unprocessed ice (Fig. S1, ESI†). The region of the most pronounced absorption (190–500 nm) can be associated with $^1A' \rightarrow {}^3A'$ transition of vinylacetylene (200–225 nm)[50] and with $\pi \rightarrow \pi^*$ transitions of (substituted) benzenes and PAHs. For example, the transition of benzene is located at 160–207 nm, and those of phenylacetylene and styrene at 215–260 nm and 220–275 nm, respectively. For polycyclic compounds, the $\pi \rightarrow \pi^*$ transitions shift to higher wavelengths with spectral ranges for naphthalene, anthracene, and phenanthrene at 245–280 nm, 300–370 nm, and 240–380 nm, respectively, whereas the pentacene transitions span the wavelength range of 290–620 nm.[51] Hence, both FTIR and UV-Vis spectra indicate the presence of cyclic aromatic molecules, but neither method allows us to assign individual aromatic molecules formed in the photochemistry. Therefore, a more selective detection method is needed to identify the product molecules and to constrain the molecular complexity achieved by the photolysis. This requirement is fulfilled by REMPI-ReToF-MS, which allows a selective detection of aromatic hydrocarbons such as benzene.

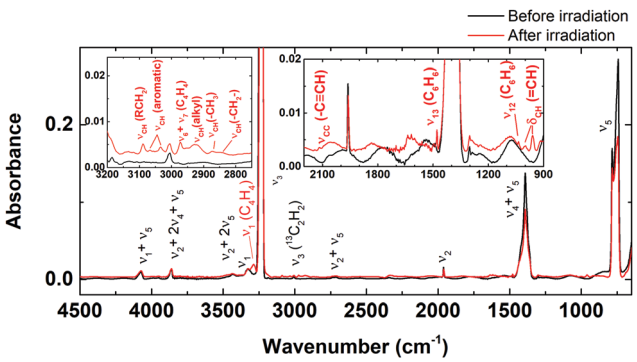

Fig. 3 Infrared spectra of acetylene ices at 5 K. Spectra were taken before (black line) and after (red line) irradiation with 222 nm photons at a dose of 8.4 ± 1.2 eV molecule^{-1}. The insets show details of the new IR bands after irradiation.

REMPI-ReToF-MS

Fig. 4 shows the temperature-dependent mass spectra of subliming molecules from the photolyzed acetylene ices recorded using the [1 + 1] REMPI scheme for benzene (C_6H_6) at 259.003 nm to ionize the desorbing molecules and to detect them in a reflectron time-of-flight mass spectrometer (ReToF-MS). REMPI first accesses an excited intermediate state, which is characteristic for the individual isomer to be identified (here: benzene) *via* a resonant photon absorption followed by a second photon, which then ionizes the molecule. As the $S_n \leftarrow S_0$ transitions of substituted benzenes and more complex PAHs can be accessed between 266 nm and 248 nm,[47] higher mass (poly)cyclic aromatics can also be detected off-resonance in the present experiments. As revealed in Fig. 4(b), PAHs with mass-to-charge ratios up to 336 ($C_{26}H_{24}$, *e.g.* dipropylperylene) carrying up to five benzene rings were detected in the experiment conducted with 249 nm photons. At 222 nm, the multichannel plate (MCP) detector of the ReToF-MS was tuned down to 3000 V, which results in below 10% sensitivity, to avoid saturation. Therefore, a lower fraction of high-mass products were detected above the noise level. An overview of the array of detected mass-to-charge ratios in the 249 nm experiment along with assignments are provided in Table S4 (ESI†); the corresponding TPD traces are shown in Fig. S2–S7 (ESI†). To quantify the production of benzene, the ion signal of m/z = 79 ($^{13}C^{12}C_5H_6$) was analyzed for each of the three experiments,

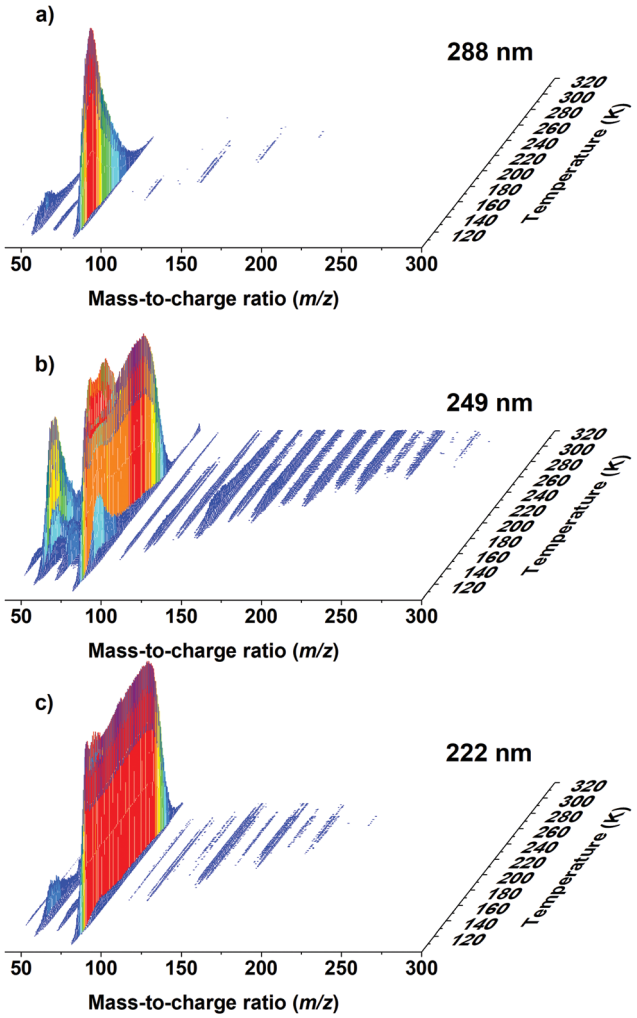

Fig. 4 Temperature-dependent mass spectra. Spectra were recorded at 259.003 nm of acetylene ices irradiated with 288 nm (top), 249 nm (middle), and 222 nm (bottom) photons.

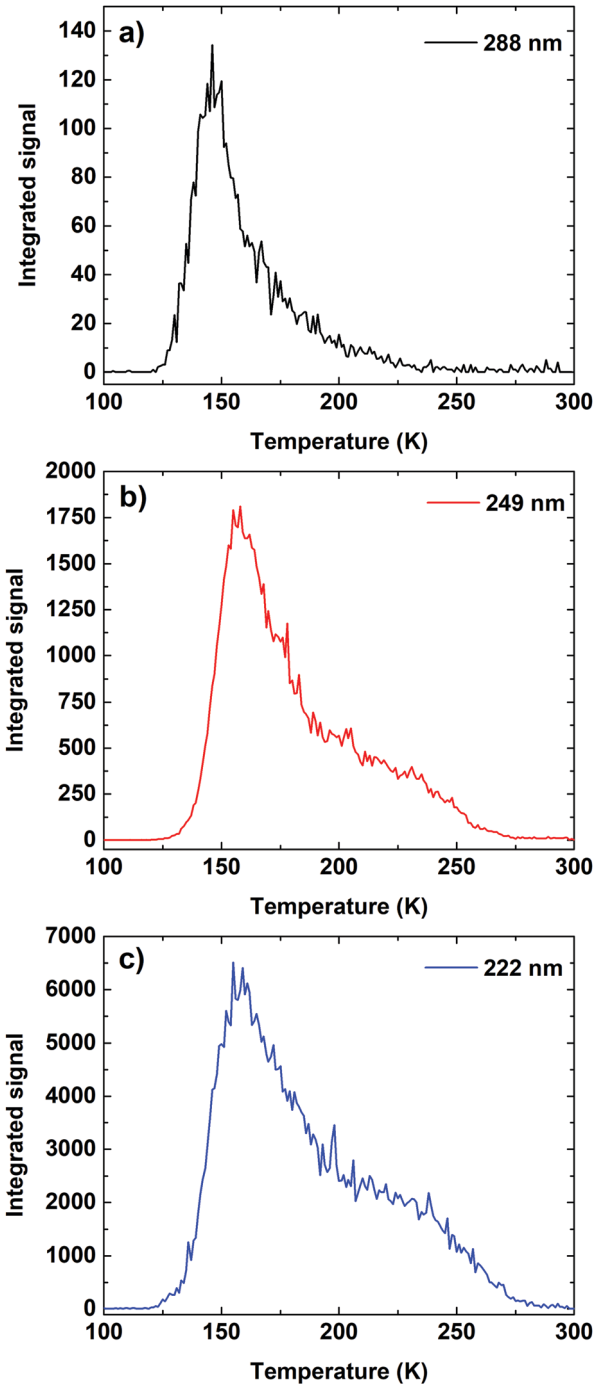

Fig. 5 TPD profiles of m/z = 79 (benzene-$^{13}C_1$). Spectra were recorded at 259.003 nm for acetylene ices irradiated with 288 nm (top), 249 nm (middle), and 222 nm (bottom) photons. The measurement of the ice photolyzed at 222 nm was recorded at a lower MCP voltage and lower ice thickness to prevent saturation and has been scaled accordingly.

because the signal at m/z = 78 was saturated due to the efficient ionization and formation of benzene. The resonance wavelength differs slightly for these two isotopologues, but benzene-$^{13}C_1$ can be efficiently detected at the resonance wavelength of benzene.[52] The resulting ion signals are displayed in Fig. 5. All traces were scaled by the number of processed molecules in the ice and by the laser power to account for fluctuations in laser pulse energy; the trace in Fig. 5c) was additionally multiplied by a factor of 10.55 to account for the reduced MCP voltage (*vide supra*). Integration over the signals yields total ion counts of 3900, 83 700, and 384 000 for 288 nm, 249 nm, and 222 nm irradiation, respectively, for benzene, *i.e.* $(3.1 \pm 0.9) \times 10^{-5}$, $(7 \pm 2) \times 10^{-4}$, and $(2.0 \pm 0.6) \times 10^{-3}$ benzene molecules per absorbed photon (ESI†). This indicates that the benzene yields increase with rising photon energy exciting to the T_1, T_2, and S_1 states (ESI†).

Electronic structure calculations

With the explicit isomer-specific identification of benzene (C_6H_6) in our laboratory experiments, we turn our attention now to possible reaction pathways by merging our experimental data with electronic structure calculations predicting relative energies of all reactants, intermediates, transition states, and products to a precision of 5 kJ mol^{-1} (Fig. 6, 7, and ESI†). It should be noted that under real planetary conditions, Pluto's surface is exposed to a broad band spectrum of low energy Solar

Photons.[8,24] Naturally, the photochemical processes cannot be explored computationally at all wavelengths for each excited state of acetylene. Therefore, as a proof-of-concept, we explore in the present study the effects of photoexcitation to the two lowest excited T_1 and T_2 states. Considering the requirement to use accurate *ab initio* electronic structure methods capable of treating excited triplet (T_1/T_2) states, we conducted first gas phase calculations. These explored the chemical response of an acetylene trimer ($(C_2H_2)_3$), which represents the minimum numbers of carbon and hydrogen atoms to form benzene, by excitation of a single acetylene molecule to the T_1 and T_2 states yielding eventually triplet benzene. At 288 nm, acetylene can only be excited to its T_1 state (Fig. 1); in the $^3B_2$ and ^3B_u states, the hydrogen atoms could either be oriented *cis* or *trans* with respect to each other. At 249 nm, the T_2 state of acetylene can be accessed; a chemical reaction can start from an acetylene in its $^3A_2$ (*cis*) and/or ^3A_u (*trans*) state; in addition, internal conversion to the T_1 state may precede prior to reaction. It should be noted that in the gas phase, singlet–triplet transitions are formally symmetry forbidden. However, for simple organic molecules such transitions are typically not strictly forbidden, which can lead to significant excitation in the solid state due to the higher density.[53]

The results of the computations reveal exciting findings. Upon excitation to T_1, *cis*-acetylene adds with a single carbon atom to the carbon–carbon double bond of a ground state acetylene molecule yielding a tricyclic ring intermediate [1] (^{3}A) (Fig. 6); this initial structure resembles a cyclopropene molecule substituted at the CH_2 moiety by a triplet carbene. In the gas phase, this addition involves a barrier of only 2 kJ mol^{-1}, which is less than the excess energy of the system (48 kJ mol^{-1}) upon excitation to the T_1 state by one 288 nm photon. [1] ring closes to an acyclic intermediate [2] (^{3}A) by passing a transition state of 35 kJ mol^{-1}, which is well below the energy of the separated reactants. Three consecutive *cis–trans* isomerizations with respect to C–H and C–C bonds involve intermediates [3] (^{3}A), [4] (^{3}A), and [5] (^{3}A); the barriers to isomerization are small (13–23 kJ mol^{-1}) and can be overcome easily. [5] can then react with another acetylene molecule through addition of one of the terminal carbon atoms of [5] to a single carbon atom of acetylene yielding an acyclic, six-carbon intermediate [6] (^{3}A), which is thermodynamically favored by 153 kJ mol^{-1} compared to [5]. Upon facile rotation around a carbon–carbon bond, [7] (^{3}A) is accessed, which eventually undergoes ring closure *via* carbon–carbon bond formation accompanied by aromatization to triplet benzene [8] ($^3B_{1u}$) in an overall exergonic reaction (−569 kJ mol^{-1}). In the ice, the latter can undergo intersystem crossing to eventually form ground state singlet benzene (C_6H_6, X^1A_1).[54]

This multistep reaction pathway is mirrored on the T_2 surface (Fig. 7). Excitation of the acetylene trimer ($(C_2H_2)_3$) in the gas phase yields an acyclic isomer [9] (^{3}A) *via* addition to a single carbon atom of a second acetylene molecule *via* a small barrier of only 6 kJ mol^{-1}, which then *trans–cis* isomerizes to intermediate [10] (^{3}A). The latter reacts with yet another acetylene molecule under simultaneous hydrogen migration to a six-carbon chain intermediate [11] (^{3}A). Two successive hydrogen shifts *via* [12] (^{3}A) access [13] (^{3}A). *trans–cis* isomerization of [13] (^{3}A) to [14] (^{3}A) followed by ring closure yields [15] (^{3}A), which contains the carbon skeleton of benzene. Two successive hydrogen shifts from the methylene moiety (CH_2) *via* [16] (^{3}A) result in triplet benzene [17] ($^3E_{1u}$). Once again, in the ice, the latter can undergo intersystem crossing to eventually form ground state singlet benzene (X^1A_1). Overall, with the exception of the initial barrier to addition of only 2 kJ mol^{-1} (T_1) and 6 kJ mol^{-1} (T_2), which range well below the excess energy

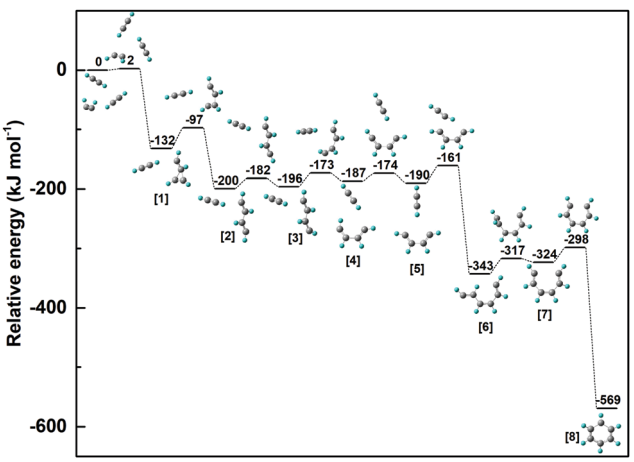

Fig. 6 The T_1 C_6H_6 potential energy surface involved in the formation of triplet benzene *via* acetylene reactions. Energies are given in kJ mol^{-1}. Geometries were optimized at the B3LYP/6-311G** level. Single-point electronic energies were calculated at the CCSD(T)/CBS level. Zero-point energies were corrected using B3LYP/6-311G**, and the solvation energy was calculated by the CPCM model with B3LYP/6-311G** (Methods section).

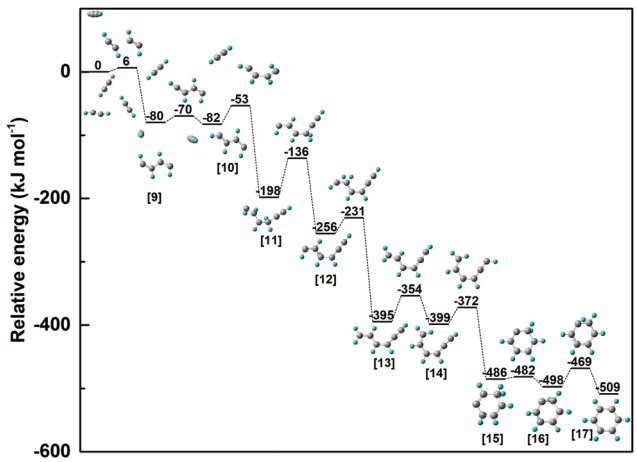

Fig. 7 The T_2 C_6H_6 potential energy surface involved in the formation of triplet benzene *via* acetylene reactions. Energies are given in kJ mol^{-1}. Geometries were optimized at the TD-B3LYP/6-311G** level. Single-point electronic energies were calculated at the CASPT2/aug-cc-pVTZ level. Zero point energies were corrected using TD-B3LYP/6-311G**, and the solvation energy was calculated by the CPCM model with TD-B3LYP/6-311G** (Methods section).

incorporated by the absorbing photons into the acetylene trimer, all barriers to yield triplet ([8] ($^3B_{1u}$) and [17] ($^3E_{1u}$) benzene are well below the energy of the separated reactants and hence can be overcome easily upon excitation of an acetylene trimer ($(C_2H_2)_3$) by a single 288 nm and 249 nm photon to the T_1 and T_2 states, respectively, in overall exergonic and 'downhill' reactions.

Since in the real ice, the acetylene trimer is surrounded by acetylene molecules, we also explored potential solvation effects and their influence on barrier heights and energies of the local minima. This is implemented by adding stepwise up to eight acetylene molecules to the acetylene trimer one molecule at a time. Considering the computationally demanding calculations, this is conducted here for the T_1 state, which can be excited in our experiments by a single 288 nm photon, as a proof-of-concept. The overall effects of the solvation on the energies of the stationary points on the T_1 surface are presented in Fig. 8. When two acetylene molecules are added to the solvation shell of the acetylene trimer, the entrance barrier decreases to 1 kJ mol^{-1}. Once a third acetylene molecule is added, at the CCSD(T)/CBS level the barrier vanishes, and the acetylene hexamer is stabilized by 0.3 kJ mol^{-1} with respect to the acetylene trimer and three separated acetylene molecules. As shown in Fig. 8, from the acetylene hexamer on, a barrier to addition to solvated [1] exists, but it is lower than the energy of the separated reactants and hence constitutes a submerged barrier in the entrance channel.

In this situation, the kinetics are controlled by two transition states: a loose, indistinct outer variational transition state and a tight inner transition state corresponding to the submerged barrier. The outer transition state is rate controlling at low temperatures. For the overall reaction from the solvated acetylene trimer to solvated [1], the reaction is *de facto* barrierless.

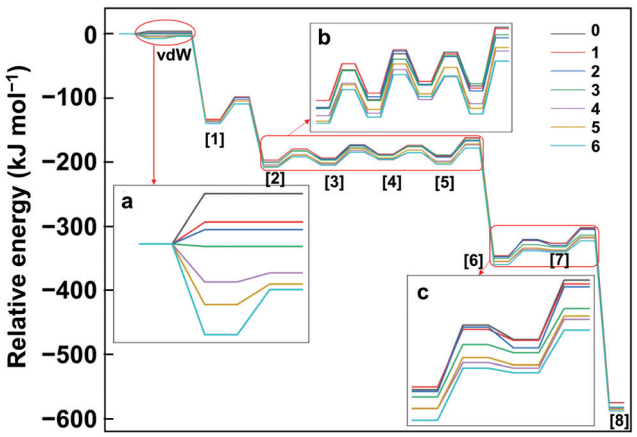

Fig. 8 Potential energy surfaces of the reaction for the formation of triplet benzene on the T_1 surface with increased number of acetylenes surrounding the benzene trimer reaction center. Relative electronic energies were calculated at the CCSD(T)/CBS level (Methods section). The legend indicates the number of additional acetylene molecules surrounding the reaction center and the transition from an entrance barrier to a submerged barrier as the number of acetylene molecules in the solvation shell increases.

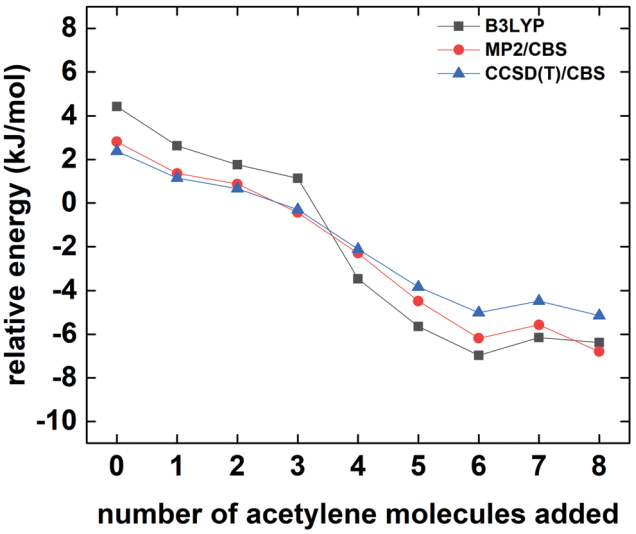

Fig. 9 Relative energies of the first transition state and/or van der Waals complex on the T_1 surface with increased number of acetylenes surrounding the benzene trimer reaction center. Energies are referenced to the initial complex as a function of the number of acetylene molecules (n) in the $C_6H_6/(C_2H_2)_n$ cluster. The energy of the initial complex is defined as zero.

Adding additional acetylene molecules to the solvation shell essentially decreases the energy of the van der Waals (vdW) cluster with overall eight acetylene molecules to 5 kJ mol^{-1} below the separated acetylene trimer and six separated acetylene molecules at the CCSD(T)/CBS level. Here, the barrier to addition lies 2 kJ mol^{-1} above the van der Waals cluster, but 3 kJ mol^{-1} below the energy of the separated reactants (see Table S9 of ESI†). From here on, adding additional acetylene molecules does not change the energy of the clusters significantly, and clusters with seven and eight acetylene molecules are essentially isoenergetic (Fig. 9).

Note that adding acetylene molecules in the solvation shell also lowers the energies of the remaining intermediates [2]–[8] and transition states among them by up to 10 kJ mol^{-1}. Overall, our computations revealed that upon solvation of the acetylene trimer, the barrier to addition forming [1] essentially submerges from the acetylene hexamer on, resulting in a barrierless reaction once a single acetylene molecule is excited to the T_1 surface forming eventually triplet benzene [8] in an energetically downhill process, which may then undergo intersystem crossing to the ground state singlet surface upon interaction with the matrix. Consequently, this one-photon excitation of acetylene suggests that the same reaction can likely occur inside the acetylene ices initiated by a single 288 nm photon even at temperatures as low as 5 K.

Discussion and conclusion

Having demonstrated that the interaction of non-ionizing radiation with acetylene ices by low-energy photons results in the formation of benzene *via de facto* barrierless and overall exergonic reaction pathways through excited state dynamics,

we now explore critical implications of these findings to Pluto's surface composition.

First, as of now, photochemical models of Pluto's atmosphere solely contain gas-phase reactions leading to the formation of benzene; the surface was assumed not to receive significant doses of radiation that can induce chemical changes eventually leading to benzene formation. Above 500 km, the main contributor for benzene formation is postulated to be the dissociative recombination of the $C_7H_7^+$ cation with an electron, *i.e.* a reaction which has not been validated in any laboratory experiment,[55] whereas below this height, the primary formation channel in the modeling is suggested to be the propargyl (C_3H_3) self-recombination ($C_3H_3 + C_3H_3 + M \rightarrow C_6H_6 + M$).[12] The latter reaction has been explored in numerous computational[56,57] and experimental studies[58–61] with benzene being a minor reaction product at a level of a few 10% at most. However, none of the research was carried out at the low temperatures and pressures found in Pluto's atmosphere. According to the theoretical models, gas phase reactions may account for a net production rate of benzene of 4×10^5 cm^{-2} s^{-1} for a total condensation of 1.6 g cm^{-2} Byr^{-1}.[12] An alternative photochemical gas-phase pathway to benzene is the reaction of three acetylene molecules. This has been studied extensively in high temperature gas phase environments for decades. The pathways involve radical-radical recombination initiated by hydrogen abstraction from the acetylene molecule possibly in conjunction with excited singlet states;[62] vacuum ultraviolet (VUV) ionization of acetylene van der Waals clusters might lead to benzene cations, but not to neutral benzene molecules.[41] Furthermore, broad band excitation of triplet states using photosensitizers like mercury has been demonstrated to yield benzene at 423–543 K, *i.e.* higher temperatures than used in this study.[63,64]

Second, in the solid state, benzene has been demonstrated to form by irradiation of acetylene ice with energetic electrons,[29,65] X-ray irradiation,[66] and cyclotrimerization on cosmic dust analogues.[67] However, the low doses reaching Pluto's surface as discussed above suggest that cosmic rays and energetic electrons, which are formed by cosmic rays decelerated through solid matter, are less important than low energy photons reaching Pluto's surface. Also, the temperature on Pluto's surface is too low for efficient cyclotrimerization of acetylene on dust and, additionally, the dust influx is too low for significant contribution of this process even at the higher temperatures found in Titan's atmosphere.[67] Previous experiments of acetylene photolysis in the solid state with VUV photons did not result in benzene formation,[68] whereas irradiation of acetylene in a xenon matrix with 248 nm photons was found to yield small amounts of benzene. However, this was attributed to excimer formation followed by energy transfer to acetylene dimers and trimers rather than a one-step excitation of the acetylene molecules.[69] The present experiments demonstrate that in the solid state, excited (triplet) state chemistry of acetylene leads to the formation of significant amounts of benzene. In contrast to one-step photo-induced cyclotrimerization by X-rays demonstrated by Lukianova and Feldman,[66] our calculations clearly indicate a multistep reaction through C_4H_4 intermediates under our experimental conditions. This is further supported by the identification of vinylacetylene in the infrared spectra, which could easily form as a final product by isomerization of the C_4H_4 intermediates. Furthermore, C_4H_4 (m/z = 52) was detected as a reaction product after irradiation of acetylene ice at 222 nm utilizing single-photon ionization at an energy of 10.49 eV (Fig. S10, ESI†). Although vinylacetylene can also form from the UV irradiation of benzene, subjecting pure benzene ices to higher doses than applied in this study did not result in detectable IR features of vinylacetylene despite the higher concentration of benzene in the ice.[70]

Third, (barrier-less) excited state reaction pathways to benzene from acetylene as demonstrated here have critical implications for the abundance of benzene along with PAHs on Pluto's surface. Owing to the low temperature on the surface (37 K), ground state acetylene molecules cannot react with each other to form benzene due to an entrance barrier of 140 kJ mol^{-1}.[65] However, as demonstrated here, low energy photoexcitation of acetylene trimers eventually yields benzene in the ices.

Fourth, Pluto's atmosphere is opaque to higher energy photons (<142.5 nm) thus making radical–radical or ion–neutral reactions of acetylene in the lower atmosphere and on the surface a minor contributor due to complete absorption of Ly-α photons and low solar emission between 142.5 nm and 215 nm. Additionally, GCRs do not deliver sufficient energy to the surface for significant chemical alteration; low energy photons exploited in the present study result in doses six orders of magnitude higher than those by GCRs. Therefore, the acetylene excited state dynamics demonstrated here represent a critical, hitherto overlooked formation route for (poly)cyclic aromatic hydrocarbons on Pluto. Especially since acetylene has been identified as the main precipitate on the surface, the formation of significant amounts of aromatics can be expected from these reactions. Considering that the highest dose used in our study corresponds to 160 ± 20 years of solar irradiation of Pluto's surface and produced an opaque yellow to golden-orange residue, significant surface coloration can be expected from excited state chemistry before the surface is covered with fresh precipitates. Furthermore, even the experiment conducted at 288 nm produced a slight, yellow residue on the sample after sublimation of volatiles. Since the dose received in these experiments corresponds to only 32 ± 4 years at the low efficiency found for 288 nm radiation, even coloration of aerosol particles in the atmosphere before they settle down on the surface could be feasible. Once benzene is formed, there are several pathways towards more complex (substituted) aromatic hydrocarbons *via* ring annulation.[29] Furthermore, benzene in the solid state subjected to long-wavelength UV radiation ($\lambda > 230$ nm) can react further to substituted benzenes such as xylene (C_8H_{10}), ethylbenzene (C_8H_{10}), and styrene (C_8H_8), which has also been detected in our experiments.[70] It is important to stress that in our experiments, PAHs carrying up to five rings and mass-to-charge ratios of 336 ($C_{26}H_{24}$, *e.g.* dipropylperylene) were detected *via* off-resonance REMPI and detected in the gas phase. The late onset of the high-mass PAH desorption (280–300 K)

indicates that this upper limit in mass is governed by product volatility rather than product formation, which is further indicated by the nonvolatile, yellowish residues after sublimation of all volatile species. Among the detected PAHs were mass-to-charge ratios that might correspond to colored PAHs such as perylene ($C_{20}H_{12}$, yellow-brown), anthanthrene ($C_{22}H_{12}$, golden yellow), and coronene ($C_{24}H_{12}$, yellow). Further mass-growth might ultimately lead to the formation of dicoronylene ($C_{48}H_{20}$, red) by fusion of two coronene molecules or to even larger coronene trimers or tetramers, which are black in color. Therefore, complex PAHs that can form from low-energy photolysis of acetylene ice span the whole range of colors found on Pluto's surface and can, alongside other photoproducts such as tholins, possibly explain the surface coloration.

Overall, the results of this study bear important implications for hydrocarbon chemistry on airless bodies or those with thin atmospheres in the Solar System. For example, Saturn's moons Phoebe and Iapetus exhibit areas of dark coloration in which Cassini detected the infrared signature of PAHs.[71,72] Especially interesting in this regard is Pluto's moon Charon. Even though it had no detectable atmosphere during the Solar occultation measurements of the New Horizons mission,[73] the polar regions exhibit a red coloration.[2] During the winter, the poles become cold enough to condense gases escaping from Pluto's atmosphere, where they can be further processed to form *e.g.* acetylene, which can later be processed by solar irradiation during the summer months, when the temperature rises high enough to sublime methane ice, hence increasing the density of the photoproducts.[74] Addition of the low energy solar radiation pathway for the formation of PAHs in the solid state could significantly increase the production rates of such coloring materials. It should be noted that the present experiments were carried out at lower temperatures (5 K) than those on the surface of Pluto (37 K) as a proof-of-concept study that is applicable to all environments. As higher temperatures increase the mobility of molecules, a favorable reaction geometry should be easier to achieve, thereby likely increasing the reaction rate. Furthermore, the overall production rate of benzene and PAHs on Pluto's surface will depend on additional factors, including acetylene concentration in the surface ice and penetration depth of the low energy solar photons. At high penetration depths, the photochemistry discussed here outweighs the benzene formation in the atmospheric models by several orders of magnitude even in dilute acetylene ices and can therefore constitute the main source of aromatic molecules on Pluto's surface therefore bringing us closer to an understanding of the coloration of Pluto's surface and of hydrocarbon-covered surfaces of airless bodies and even those with an atmosphere like Triton (as long as the low energy photons can penetrate to the surface) in our Solar System in general.

Author contributions

RIK designed the experiment. NFK and AMT carried out the experimental measurements. J-IL and B-MC performed the thin film absorption measurements. NFK performed the data analyses. YW, CC, TY and XH performed theoretical calculations and data analyses. NFK, LAY, and RIK wrote the manuscript. YWL and C-HC performed the theoretical calculations. TY and XH supervised the theoretical calculations. All authors discussed the data and the manuscript.

Conflicts of interest

There are no conflicts to declare.

Acknowledgements

The W. M. Keck Foundation and the University of Hawaii at Manoa financed the construction of the experimental setup. We also thank the Supercomputer Center of East China Normal University (ECNU Multifunctional Platform for Innovation 001) for providing computer resources. Special thanks to Prof. Robert Field (MIT) and the New Horizons Science Team for stimulating discussions. The experimental research at the University of Hawaii was supported by the US National Science Foundation (NSF), Division for Astronomy (NSF-AST 1800975) (NFK, AMT, RIK). NFK acknowledges funding from the Deutsche Forschungsgemeinschaft (DFG, German Research Foundation) for a postdoctoral fellowship (KL 3342/1-1). XH acknowledges the National Natural Science Foundation of China (Grant No. 21922301, 21761132022 and 21673074), the National Key R&D Program of China (Grant No. 2016YFA0501700 and 2019YFA0905201), and Shanghai Municipal Natural Science Foundation (Grant No. 18ZR1412600). TY thanks the support from the National Natural Science Foundation of China (Grant No. 12034008 and 11874151), the projects from Shanghai Science and Technology Commission (Grant No. 19JC1412200), the Young Top-Notch Talent Support Program of Shanghai and the Program for Professor of Special Appointment (Eastern Scholar) at Shanghai Institutions of Higher Learning. Both XH and TY acknowledge the Fundamental Research Funds for the Central Universities. B-MC thanks for the support from Ministry of Science and Technology of Taiwan (grant 109-2113-M-303-001) and NSRRC for providing the beamline and instruments for the measurement of absorption.

References

1 J. M. Moore, W. B. McKinnon, J. R. Spencer, A. D. Howard, P. M. Schenk, R. A. Beyer, F. Nimmo, K. N. Singer, O. M. Umurhan, O. L. White, S. A. Stern, K. Ennico, C. B. Olkin, H. A. Weaver, L. A. Young, R. P. Binzel, M. W. Buie, B. J. Buratti, A. F. Cheng, D. P. Cruikshank, W. M. Grundy, I. R. Linscott, H. J. Reitsema, D. C. Reuter, M. R. Showalter, V. J. Bray, C. L. Chavez, C. J. A. Howett, T. R. Lauer, C. M. Lisse, A. H. Parker, S. B. Porter, S. J. Robbins, K. Runyon, T. Stryk, H. B. Throop,

C. C. C. Tsang, A. J. Verbiscer, A. M. Zangari, A. L. Chaikin and D. E. Wilhelms, *Science*, 2016, **351**, 1284.
2 W. M. Grundy, R. P. Binzel, B. J. Buratti, J. C. Cook, D. P. Cruikshank, C. M. Dalle Ore, A. M. Earle, K. Ennico, C. J. A. Howett, A. W. Lunsford, C. B. Olkin, A. H. Parker, S. Philippe, S. Protopapa, E. Quirico, D. C. Reuter, B. Schmitt, K. N. Singer, A. J. Verbiscer, R. A. Beyer, M. W. Buie, A. F. Cheng, D. E. Jennings, I. R. Linscott, J. W. Parker, P. M. Schenk, J. R. Spencer, J. A. Stansberry, S. A. Stern, H. B. Throop, C. C. C. Tsang, H. A. Weaver, G. E. Weigle and L. A. Young, *Science*, 2016, **351**, aad9189.
3 A. D. Howard, J. M. Moore, O. M. Umurhan, O. L. White, R. S. Anderson, W. B. McKinnon, J. R. Spencer, P. M. Schenk, R. A. Beyer, S. A. Stern, K. Ennico, C. B. Olkin, H. A. Weaver and L. A. Young, *Icarus*, 2017, **287**, 287–300.
4 M. W. Telfer, E. J. R. Parteli, J. Radebaugh, R. A. Beyer, T. Bertrand, F. Forget, F. Nimmo, W. M. Grundy, J. M. Moore, S. A. Stern, J. Spencer, T. R. Lauer, A. M. Earle, R. P. Binzel, H. A. Weaver, C. B. Olkin, L. A. Young, K. Ennico and K. Runyon, *Science*, 2018, **360**, 992.
5 J. M. Moore, A. D. Howard, O. M. Umurhan, O. L. White, P. M. Schenk, R. A. Beyer, W. B. McKinnon, J. R. Spencer, W. M. Grundy, T. R. Lauer, F. Nimmo, L. A. Young, S. A. Stern, H. A. Weaver, C. B. Olkin and K. Ennico, *Icarus*, 2017, **287**, 320–333.
6 J. E. Moores, C. L. Smith, A. D. Toigo and S. D. Guzewich, *Nature*, 2017, **541**, 188–190.
7 L. A. Young, J. A. Kammer, A. J. Steffl, G. R. Gladstone, M. E. Summers, D. F. Strobel, D. P. Hinson, S. A. Stern, H. A. Weaver, C. B. Olkin, K. Ennico, D. J. McComas, A. F. Cheng, P. Gao, P. Lavvas, I. R. Linscott, M. L. Wong, Y. L. Yung, N. Cunningham, M. Davis, J. W. Parker, E. Schindhelm, O. H. W. Siegmund, J. Stone, K. Retherford and M. Versteeg, *Icarus*, 2018, **300**, 174–199.
8 G. R. Gladstone, S. A. Stern, K. Ennico, C. B. Olkin, H. A. Weaver, L. A. Young, M. E. Summers, D. F. Strobel, D. P. Hinson, J. A. Kammer, A. H. Parker, A. J. Steffl, I. R. Linscott, J. W. Parker, A. F. Cheng, D. C. Slater, M. H. Versteeg, T. K. Greathouse, K. D. Retherford, H. Throop, N. J. Cunningham, W. W. Woods, K. N. Singer, C. C. C. Tsang, E. Schindhelm, C. M. Lisse, M. L. Wong, Y. L. Yung, X. Zhu, W. Curdt, P. Lavvas, E. F. Young and G. L. Tyler, *Science*, 2016, **351**, aad8866.
9 A. J. Steffl, L. A. Young, D. F. Strobel, J. A. Kammer, J. S. Evans, M. H. Stevens, R. N. Schindhelm, J. W. Parker, S. A. Stern, H. A. Weaver, C. B. Olkin, K. Ennico, J. R. Cummings, G. R. Gladstone, T. K. Greathouse, D. P. Hinson, K. D. Retherford, M. E. Summers and M. Versteeg, *Astron. J.*, 2020, **159**, 274.
10 E. Lellouch, M. Gurwell, B. Butler, T. Fouchet, P. Lavvas, D. F. Strobel, B. Sicardy, A. Moullet, R. Moreno, D. Bockelée-Morvan, N. Biver, L. Young, D. Lis, J. Stansberry, A. Stern, H. Weaver, E. Young, X. Zhu and J. Boissier, *Icarus*, 2017, **286**, 289–307.
11 M. L. Wong, S. Fan, P. Gao, M.-C. Liang, R.-L. Shia, Y. L. Yung, J. A. Kammer, M. E. Summers, G. R. Gladstone, L. A. Young, C. B. Olkin, K. Ennico, H. A. Weaver and S. A. Stern, *Icarus*, 2017, **287**, 110–115.
12 V. A. Krasnopolsky, *Icarus*, 2020, **335**, 113374.
13 A. Luspay-Kuti, K. Mandt, K.-L. Jessup, J. Kammer, V. Hue, M. Hamel and R. Filwett, *Mon. Not. R. Astron. Soc.*, 2017, **472**, 104–117.
14 P. M. Schenk, R. A. Beyer, W. B. McKinnon, J. M. Moore, J. R. Spencer, O. L. White, K. Singer, F. Nimmo, C. Thomason, T. R. Lauer, S. Robbins, O. M. Umurhan, W. M. Grundy, S. A. Stern, H. A. Weaver, L. A. Young, K. E. Smith and C. Olkin, *Icarus*, 2018, **314**, 400–433.
15 W. M. Grundy, T. Bertrand, R. P. Binzel, M. W. Buie, B. J. Buratti, A. F. Cheng, J. C. Cook, D. P. Cruikshank, S. L. Devins, C. M. Dalle Ore, A. M. Earle, K. Ennico, F. Forget, P. Gao, G. R. Gladstone, C. J. A. Howett, D. E. Jennings, J. A. Kammer, T. R. Lauer, I. R. Linscott, C. M. Lisse, A. W. Lunsford, W. B. McKinnon, C. B. Olkin, A. H. Parker, S. Protopapa, E. Quirico, D. C. Reuter, B. Schmitt, K. N. Singer, J. A. Spencer, S. A. Stern, D. F. Strobel, M. E. Summers, H. A. Weaver, G. E. Weigle, M. L. Wong, E. F. Young, L. A. Young and X. Zhang, *Icarus*, 2018, **314**, 232–245.
16 S. Protopapa, C. B. Olkin, W. M. Grundy, J.-Y. Li, A. Verbiscer, D. P. Cruikshank, T. Gautier, E. Quirico, J. C. Cook, D. Reuter, C. J. A. Howett, A. Stern, R. A. Beyer, S. Porter, L. A. Young, H. A. Weaver, K. Ennico, C. M. Dalle Ore, F. Scipioni and K. Singer, *Astron. J.*, 2020, **159**, 74.
17 F. Scipioni, O. White, J. C. Cook, T. Bertrand, D. P. Cruikshank, W. M. Grundy, C. Beddingfield-Cartwright, R. P. Binzel, C. M. Dalle Ore, D. Jennings, J. M. Moore, C. B. Olkin, S. Protopapa, D. C. Reuter, B. Schmitt, K. N. Singer, J. R. Spencer, S. A. Stern, H. A. Weaver, A. J. Verbiscer and L. A. Young, *Icarus*, 2021, **359**, 114303.
18 A. F. Cheng, M. E. Summers, G. R. Gladstone, D. F. Strobel, L. A. Young, P. Lavvas, J. A. Kammer, C. M. Lisse, A. H. Parker, E. F. Young, S. A. Stern, H. A. Weaver, C. B. Olkin and K. Ennico, *Icarus*, 2017, **290**, 112–133.
19 P. Gao, S. Fan, M. L. Wong, M.-C. Liang, R.-L. Shia, J. A. Kammer, Y. L. Yung, M. E. Summers, G. R. Gladstone, L. A. Young, C. B. Olkin, K. Ennico, H. A. Weaver and S. A. Stern, *Icarus*, 2017, **287**, 116–123.
20 P. Lavvas, E. Lellouch, D. F. Strobel, M. A. Gurwell, A. F. Cheng, L. A. Young and G. R. Gladstone, *Nat. Astron.*, 2021, **5**, 289–297.
21 T. Bertrand, F. Forget, O. M. Umurhan, J. M. Moore, L. A. Young, S. Protopapa, W. M. Grundy, B. Schmitt, R. D. Dhingra, R. P. Binzel, A. M. Earle, D. P. Cruikshank, S. A. Stern, H. A. Weaver, K. Ennico and C. B. Olkin, *Icarus*, 2019, **329**, 148–165.
22 P. E. Johnson, L. A. Young, S. Protopapa, B. Schmitt, L. R. Gabasova, B. L. Lewis, J. A. Stansberry, K. E. Mandt and O. L. White, *Icarus*, 2021, **356**, 114070.
23 R. E. Johnson, *GeoRL*, 1989, **16**, 1233–1236.
24 X. Zhang, D. F. Strobel and H. Imanaka, *Nature*, 2017, **551**, 352–355.
25 V. A. Krasnopolsky, *Icarus*, 2014, **236**, 83–91.

26 B. M. Jones and R. I. Kaiser, *JPCL*, 2013, **4**, 1965–1971.
27 A. M. Turner, M. J. Abplanalp, S. Y. Chen, Y. T. Chen, A. H. H. Chang and R. I. Kaiser, *Phys. Chem. Chem. Phys.*, 2015, **17**, 27281–27291.
28 R. L. Hudson, R. F. Ferrante and M. H. Moore, *Icarus*, 2014, **228**, 276–287.
29 M. J. Abplanalp, R. Frigge and R. I. Kaiser, *Sci. Adv.*, 2019, **5**, eaaw5841.
30 H.-C. Lu, H.-K. Chen, B.-M. Cheng and J. F. Ogilvie, *Spectrochim. Acta, Part A*, 2008, **71**, 1485–1491.
31 Y.-P. Kuo, H.-C. Lu, Y.-J. Wu, B.-M. Cheng and J. F. Ogilvie, *Chem. Phys. Lett.*, 2007, **447**, 168–174.
32 A. D. Becke, *J. Chem. Phys.*, 1993, **98**, 5648–5652.
33 K. Raghavachari, G. W. Trucks, J. A. Pople and M. Head-Gordon, *Chem. Phys. Lett.*, 1989, **157**, 479–483.
34 A. Halkier, T. Helgaker, P. Jørgensen, W. Klopper, H. Koch, J. Olsen and A. K. Wilson, *Chem. Phys. Lett.*, 1998, **286**, 243–252.
35 M. J. Frisch, G. W. Trucks, H. B. Schlegel, G. E. Scuseria, M. A. Robb, J. R. Cheeseman, G. Scalmani, V. Barone, B. Mennucci, G. A. Petersson, H. Nakatsuji, M. Caricato, X. Li, H. P. Hratchian, A. F. Izmaylov, J. Bloino, G. Zheng, J. L. Sonnenberg, M. Hada, M. Ehara, K. Toyota, R. Fukuda, J. Hasegawa, M. Ishida, T. Nakajima, Y. Honda, O. Kitao, H. Nakai, T. Vreven, J. A. Montgomery, Jr., J. E. Peralta, F. Ogliaro, M. Bearpark, J. J. Heyd, E. Brothers, K. N. Kudin, V. N. Staroverov, R. Kobayashi, J. Normand, K. Raghavachari, A. Rendell, J. C. Burant, S. S. Iyengar, J. Tomasi, M. Cossi, N. Rega, J. M. Millam, M. Klene, J. E. Knox, J. B. Cross, V. Bakken, C. Adamo, J. Jaramillo, R. Gomperts, R. E. Stratmann, O. Yazyev, A. J. Austin, R. Cammi, C. Pomelli, J. W. Ochterski, R. L. Martin, K. Morokuma, V. G. Zakrzewski, G. A. Voth, P. Salvador, J. J. Dannenberg, S. Dapprich, A. D. Daniels, Ö. Farkas, J. B. Foresman, J. V. Ortiz, J. Cioslowski and D. J. Fox, *Gaussian 09, Revision C.01*, Gaussian, Inc., Wallingford CT, USA, 2009.
36 H.-J. Werner, P. J. Knowles, G. Knizia, F. R. Manby and M. Schütz, *Wiley Interdiscip. Rev. Comput. Mol. Sci.*, 2012, **2**, 242–253.
37 M. J. Frisch, G. W. Trucks, H. B. Schlegel, G. E. Scuseria, M. A. Robb, J. R. Cheeseman, G. Scalmani, V. Barone, G. A. Petersson, H. Nakatsuji, X. Li, M. Caricato, A. Marenich, J. Bloino, B. G. Janesko, R. Gomperts, B. Mennucci, H. P. Hratchian, J. V. Ortiz, A. F. Izmaylov, J. L. Sonnenberg, D. Williams-Young, F. Ding, F. Lipparini, F. Egidi, J. Goings, B. Peng, A. Petrone, T. Henderson, D. Ranasinghe, V. G. Zakrzewski, J. Gao, N. Rega, G. Zheng, W. Liang, M. Hada, M. Ehara, K. Toyota, R. Fukuda, J. Hasegawa, M. Ishida, T. Nakajima, Y. Honda, O. Kitao, H. Nakai, T. Vreven, K. Throssell, J. A. Montgomery, Jr., J. E. Peralta, F. Ogliaro, M. Bearpark, J. J. Heyd, E. Brothers, K. N. Kudin, V. N. Staroverov, T. Keith, R. Kobayashi, J. Normand, K. Raghavachari, A. Rendell, J. C. Burant, S. S. Iyengar, J. Tomasi, M. Cossi, J. M. Millam, M. Klene, C. Adamo, R. Cammi, J. W. Ochterski, R. L. Martin, K. Morokuma, O. Farkas, J. B. Foresman and D. J. Fox, *Gaussian 16, Revision A.03*, Gaussian, Inc., Wallingford CT, USA, 2016.
38 P. Celani and H.-J. Werner, *J. Chem. Phys.*, 2000, **112**, 5546–5557.
39 S. J. Blanksby and G. B. Ellison, *Acc. Chem. Res.*, 2003, **36**, 255–263.
40 R. A. Mackie, S. W. J. Scully, A. M. Sands, R. Browning, K. F. Dunn and C. J. Latimer, *Int. J. Mass Spectrom.*, 2003, **223–224**, 67–79.
41 T. Stein, B. Bandyopadhyay, T. P. Troy, Y. Fang, O. Kostko, M. Ahmed and M. Head-Gordon, *Proc. Natl. Acad. Sci. U. S. A.*, 2017, **114**, E4125.
42 M. Ahmed and A. B. Callear, *Chem. Phys. Lett.*, 1989, **156**, 35–38.
43 J. K. G. Watson, M. Herman, J. C. Van Craen and R. Colin, *JMoSp*, 1982, **95**, 101–132.
44 E. Ventura, M. Dallos and H. Lischka, *J. Chem. Phys.*, 2003, **118**, 1702–1713.
45 K. Malsch, R. Rebentisch, P. Swiderek and G. Hohlneicher, *Theor. Chem. Acc.*, 1998, **100**, 171–182.
46 R. Swanepoel, *J. Phys. E: Sci. Instrum.*, 1983, **16**, 1214–1222.
47 T. Streibel and R. Zimmermann, *Annu. Rev. Anal. Chem.*, 2014, **7**, 361–381.
48 J. Mouzay, I. Couturier-Tamburelli, N. Piétri and T. Chiavassa, *J. Geophys. Res.: Planets*, 2021, **126**, e2020JE006566.
49 Y. S. Kim and R. I. Kaiser, *ApJS*, 2009, **181**, 543–547.
50 A. Fahr and A. Nayak, *ChPh*, 1996, **203**, 351–358.
51 S. G. Lias, J. E. Bartmess, J. F. Liebman, J. L. Holmes, R. D. Levin, W. G. Mallard and S. A. Kafafi, *NIST Chemistry WebBook, NIST Standard Reference Database Number 69*, National Institute of Standards and Technology, Gaithersburg, MD, 2021.
52 U. Boesl, H. J. Neusser and E. W. Schlag, *Z. Naturforsch. A*, 1978, **33**, 1546–1548.
53 J. R. Platt, *J. Opt. Soc. Am.*, 1953, **43**, 252–257.
54 R. B. Cundall, D. A. Robinson and L. C. Pereira, in *Advances in Photochemistry*, ed. J. N. Pitts, Jr., G. S. Hammond and K. Gollnick, John Wiley & Sons, 1977, vol. 10, pp. 147–219.
55 J. C. Loison, M. Dobrijevic and K. M. Hickson, *Icarus*, 2019, **329**, 55–71.
56 J. A. Miller and C. F. Melius, *CoFl*, 1992, **91**, 21–39.
57 J. A. Miller and S. J. Klippenstein, *J. Phys. Chem. A*, 2001, **105**, 7254–7266.
58 C. L. Morter, S. K. Farhat, J. D. Adamson, G. P. Glass and R. F. Curl, *JPhCh*, 1994, **98**, 7029–7035.
59 P.-T. Howe and A. Fahr, *J. Phys. Chem. A*, 2003, **107**, 9603–9610.
60 W. Tang, R. S. Tranter and K. Brezinsky, *J. Phys. Chem. A*, 2005, **109**, 6056–6065.
61 L. Zhao, W. Lu, M. Ahmed, M. V. Zagidullin, V. N. Azyazov, A. N. Morozov, A. M. Mebel and R. I. Kaiser, *Sci. Adv.*, 2021, **7**, eabf0360.
62 M. Zelikoff and L. M. Aschenbrand, *J. Chem. Phys.*, 1956, **24**, 1034–1037.

63 S. Tsunashima and S. Sato, *Bull. Chem. Soc. Jpn.*, 1968, **41**, 2281–2284.
64 S. Shida and M. Tsukada, *Bull. Chem. Soc. Jpn.*, 1970, **43**, 2740–2745.
65 L. Zhou, W. Zheng, R. I. Kaiser, A. Landera, A. M. Mebel, M. C. Liang and Y. L. Yung, *Astrophys. J.*, 2010, **718**, 1243–1251.
66 M. A. Lukianova and V. I. Feldman, *RaPC*, 2021, **183**, 109417.
67 V. L. Frankland, A. D. James, J. D. C. Sánchez, T. P. Mangan, K. Willacy, A. R. Poppe and J. M. C. Plane, *Icarus*, 2016, **278**, 88–99.
68 S. H. Cuylle, D. Zhao, G. Strazzulla and H. Linnartz, *A&A*, 2014, **570**, 1–11.
69 G. Maier and C. Lautz, *Eur. J. Org. Chem.*, 1998, 769–776.
70 J. Mouzay, K. Henry, A. Ruf, I. Couturier-Tamburelli, G. Danger, N. Piétri and T. Chiavassa, *Planet. Sci. J.*, 2021, **2**, 37.
71 D. P. Cruikshank, C. M. Dalle Ore, R. N. Clark and Y. J. Pendleton, *Icarus*, 2014, **233**, 306–315.
72 B. J. Buratti, K. Soderlund, J. Bauer, J. A. Mosher, M. D. Hicks, D. P. Simonelli, R. Jaumann, R. N. Clark, R. H. Brown, D. P. Cruikshank and T. Momary, *Icarus*, 2008, **193**, 309–322.
73 S. A. Stern, J. A. Kammer, G. R. Gladstone, A. J. Steffl, A. F. Cheng, L. A. Young, H. A. Weaver, C. B. Olkin, K. Ennico, J. W. Parker, A. H. Parker, T. R. Lauer, A. Zangari and M. Summers, *Icarus*, 2017, **287**, 124–130.
74 W. M. Grundy, D. P. Cruikshank, G. R. Gladstone, C. J. A. Howett, T. R. Lauer, J. R. Spencer, M. E. Summers, M. W. Buie, A. M. Earle, K. Ennico, J. W. Parker, S. B. Porter, K. N. Singer, S. A. Stern, A. J. Verbiscer, R. A. Beyer, R. P. Binzel, B. J. Buratti, J. C. Cook, C. M. Dalle Ore, C. B. Olkin, A. H. Parker, S. Protopapa, E. Quirico, K. D. Retherford, S. J. Robbins, B. Schmitt, J. A. Stansberry, O. M. Umurhan, H. A. Weaver, L. A. Young, A. M. Zangari, V. J. Bray, A. F. Cheng, W. B. McKinnon, R. L. McNutt, J. M. Moore, F. Nimmo, D. C. Reuter, P. M. Schenk, S. A. Stern, F. Bagenal, K. Ennico, G. R. Gladstone, W. M. Grundy, W. B. McKinnon, J. M. Moore, C. B. Olkin, J. R. Spencer, H. A. Weaver, L. A. Young, T. Andert, O. Barnouin, R. A. Beyer, R. P. Binzel, M. Bird, V. J. Bray, M. Brozović, M. W. Buie, B. J. Buratti, A. F. Cheng, J. C. Cook, D. P. Cruikshank, C. M. Dalle Ore, A. M. Earle, H. A. Elliott, T. K. Greathouse, M. Hahn, D. P. Hamilton, M. E. Hill, D. P. Hinson, J. Hofgartner, M. Horányi, A. D. Howard, C. J. A. Howett, D. E. Jennings, J. A. Kammer, P. Kollmann, T. R. Lauer, P. Lavvas, I. R. Linscott, C. M. Lisse, A. W. Lunsford, D. J. McComas, R. L. McNutt Jr, M. Mutchler, F. Nimmo, J. I. Nunez, M. Paetzold, A. H. Parker, J. W. Parker, S. Philippe, M. Piquette, S. B. Porter, S. Protopapa, E. Quirico, H. J. Reitsema, D. C. Reuter, S. J. Robbins, J. H. Roberts, K. Runyon, P. M. Schenk, E. Schindhelm, B. Schmitt, M. R. Showalter, K. N. Singer, J. A. Stansberry, A. J. Steffl, D. F. Strobel, T. Stryk, M. E. Summers, J. R. Szalay, H. B. Throop, C. C. C. Tsang, G. L. Tyler, O. M. Umurhan, A. J. Verbiscer, M. H. Versteeg, G. E. Weigle Ii, O. L. White, W. W. Woods, E. F. Young, A. M. Zangari and The New Horizons Science Team, *Nature*, 2016, **539**, 65–68.

